Mechanical Research of Carbon Nanotubes/PMMA Composite Films

Jen-Tsung Luo,[1] **Hua-Chiang Wen,**[1] **Wen-Fa Wu,**[2] **Chang-Pin Chou**[1]

[1]*Department of Mechanical Engineering, National Chiao Tung University, Hsinchu, Taiwan*

[2]*National Nano Device Laboratories, Hsinchu, Taiwan*

Carbon nanotubes (CNTs) are one of the best candidates for reinforcing the next generation of high-performance nanocomposites owing to their excellent mechanical properties. In this study, CNTs were dispersed in polymethymethacrylate (PMMA) gel to enhance its mechanical strength. CNTs/PMMA composite films were fabricated using direct mixing and sonication. FTIR was utilized to observe the chemical structure and functional groups of the material components. The morphological feature and phase structure were observed via scanning electron microscope. A nanoindenter system was also applied to investigate the mechanical properties of composite films by a conventional method. CNTs were chemically treated by immersing them in acidic solutions to ensure extensive dispersion in the surrounding matrix. Most of the CNTs were dispersed uniformly therein. The effective dispersion of CNTs improves the mechanical performance of the composite film, wheras the poor dispersion reduces the performance. The solvent, solubility and attractive intermolecular forces, such as hydrogen bonds and Van Der Waal forces affect the dispersion of the CNTs. The carbonyl group, which was found on the composite film, contributed to the formation of a covalent bond between PMMA and the CNTs. The mechanical interaction between CNTs and the polymer was very complex. It was also governed by the interface interaction. The mechanical properties of the composite films improved as the concentration of CNTs increased. POLYM. COMPOS., 29:1285–1290, 2008. © 2008 Society of Plastics Engineers

INTRODUCTION

Polymethymethacrylate (PMMA) has been extensively employed because of their potential applications in light emitting devices, batteries, optics, electromagnetic shielding, corrosion-resistant coatings, and many applications [1–5]. However, their poor mechanical strength limits their range of applications. Nanoscale reinforcement is considered to improve the mechanical and electrical performance of PMMA effectively. Recently, carbon nanotubes (CNTs) have been effectively used as fillers in nanocomposites in scientific and technical applications. They have an elastic modulus and a tensile strength of over 1.8 TPa and 50 GPa, respectively, whose values significantly exceed those of PMMA [6–8]. CNTs also have a large surface area/volume ratio, associated with a large contact area between the filler and the matrix. The excellent mechanical and electrical properties of CNTs are expected to improve the corresponding properties of PMMA materials.

Improvements to CNTs/PMMA composites have been made in recent years. Gorga and Cohen discussed the mechanical properties of CNTs/PMMA nanocomposites as a function of the orientation, length, and concentration of nanotubes. They found that 1 wt% CNTs in PMMA increased the modulus and yield strength by 38 and 25%, respectively [9]. Sabba and Thomas employed a novel approach, based on treating single-wall carbon nanotubes (SWCNTs) with a solution of hydroxylamine hydrochloric acid salt, to disperse SWCNTs that can be easily be incorporated into an organic matrix [10]. Yang et al. constructed CNTs/PMMA nanocomposites using in situ polymerization process. CNTs were found dramatically to reduce friction and improve the wear resistance of nanocomposites [11]. Jia et al. also adopted an in situ process to compound CNTs in a PMMA matrix. The π-bonds were opened by the initiator (2,2-azobisisobutyronitrile(AIBN)) and the dangling bonds may participate in PMMA polymerization, forming a strong combining interface between the CNTs and the PMMA matrix [12].

To achieve the predict improvement, CNTs must be well dispersed into the matrix and connected to the molecular of matrix using an modified terminal bond to prevent slipping and enable the loading force transferring from matrix to the filler. Unfortunately, CNTs are difficult to disperse well in organic solvent, because of their high surface area/volume ratio resulted in a large Van Der Waals attraction and let them aggregate together. So, purification and polarization

treatments were needed to make CNTs perform well and disperse uniformly. For optimal performance in reinforcing application, CNTs should be separated into individual or bundles of only a few tubes. There are several methods to have CNTs be functionalized, such as covalence or noncovalence method, sonication technology, surfactant addition, and chemical modification [13–18]. Acid solutions are common reagents for surface purification and terminal oxidation of CNTs. They also have the ability to remove metal catalysts and together with some of the amorphous carbon [19, 20]. Acid solution with reflux or sonication can also open the ends of the CNTs and introduced carboxylic acid group [21–26]. The carboxyl group played an important role for CNTs reacting with organic matrix and making them bound tightly [27].

In this study, acid treatment methods were adopted to identify factors that can affect the dispersal of nanotubes in a PMMA matrix. The physical and chemical characteristics of CNTs /PMMA composite films were examined using FTIR, thermal desorption spectrometer (TDS), scanning electron microscope (SEM) and a nanoindenter system.

EXPERIMENT

Multi-walled carbon nanotubes (MWCNTs) were grown on a cobalt catalyst by thermal chemical vapor deposition at 600°C in a quartz tube furnace. The as-deposited carbon nanotubes were attached to acid solutions to be polarized by the following procedure. 500 mg of CNTs were immersed in various acidic solutions, including HCl (2 M), HNO$_3$ (4 M), and H$_2$SO$_4$/HNO$_3$ (3/1 by volume). The mixtures were placed in a reflux system for 24 h and then sonicated in a bath for 3 h at room temperature. Then, they were diluted by adding deionized water until the pH value was neutral, before being filtered through a membrane with 0.2 μm pores. A suspension of oxidized CNTs in ethanol was sonicated for 30 min; slowly dispersed in methyl methacrylate resin, and manually stirred until the solvent evaporated. A CNTs/methyl methacrylate mixture was then mixed with 2% of initiator (AIBN). Then, the precursor was placed on a hotplate at a temperature of 60°C to synthesize the polymer. A Teflon rod was used to stir the solution manually. Then, the solution was spin-coated on silicon or glass substrates. Following baking at 50°C for 24 h, composite films with filler concentrations from 0 to 5 wt% were prepared.

The thickness and morphology of the films was observed using a HITACHI S-4000 SEM. Fourier transform infrared spectroscopy (FTIR, ASTeX PDS-17 System) was conducted using a CsI laser source with a resolution of 4 cm^{-1}, scanning from 400 to 4000 cm^{-1}. The spectrum was obtained with an average of 32 scans. A TDS was utilized to monitor the desorption amount of methyl, carbon dioxide, and oxygen. The nanoindentation test was conducted with a commercially available machine, Nano Indenter XP System, supplied by MTS Company. The force and displacement resolutions of the nanoindenter are 500 nN and 0.1 nm, respectively. The indenter was a triangular pyra-
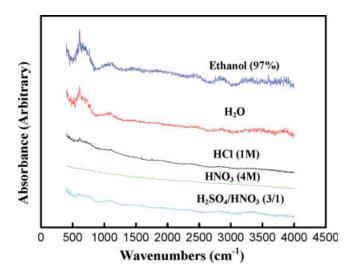

FIG. 1. FTIR spectras of CNTs immersed in different solutions. [Color figure can be viewed in the online issue, which is available at www.interscience.wiley.com.]

mid-shaped diamond with an edge angle of about 115° (Berkovich indnter). The nanoindentation test was repeated 10 times under each condition. Then, the load-penetration depth curve was recorded.

RESULTS AND DISCUSSION

Figure 1 presents the FTIR spectra of acid-treated CNTs. The peak at 1700–1750 cm^{-1} corresponds to the carboxyl group (COO$^-$). The peak at 1580 cm^{-1} is the carbonyl (C=O) group. The carboxyl group is suggested to have been introduced on the surface of CNTs after acid treatment, grafting mainly onto the area of defects and the open end of the tube. The spectra of samples that were immersed in H$_2$O or ethanol solution suffered from noise, suggesting that such impurities as metal catalyst, amorphous carbon and residual alkane or alkyne, remained on the surface of the CNTs. Acid treatment makes the surface of the nanotubes more hydrophilic. The intensity of the Van der Waals force was reduced and the self-aggregation of CNTs also reduced. Acid treatment also helped to separate and cut tubes, helping to disperse them more uniformly [28].

Polyaniline was obtained via interfacial polymerization [29]. Figure 2 displays SEM images. Fig. 2a depicts the cross-sectional morphology of pure PMMA. The thickness of the film was about 3 μm. The PMMA resin was uniformly coated on the silicon wafer. Some interfacial voids were present on the interface. Figure 2b is the surface image of a CNTs/PMMA composite film that had not been mechanically polished. The surface was smooth and CNTs were embedded in the matrix. Figure 2c and d show high-magnification images of mechanically polished composite films, obtained after the CNTs were treated using H$_2$SO$_4$/HNO$_3$ solution. CNTs were dispersed uniformly in the surrounding matrix. The carboxyl acid groups on the CNTs promote the interaction and increase the compatibility of the polymer with the CNTs. The CNTs were curved and interwoven because of
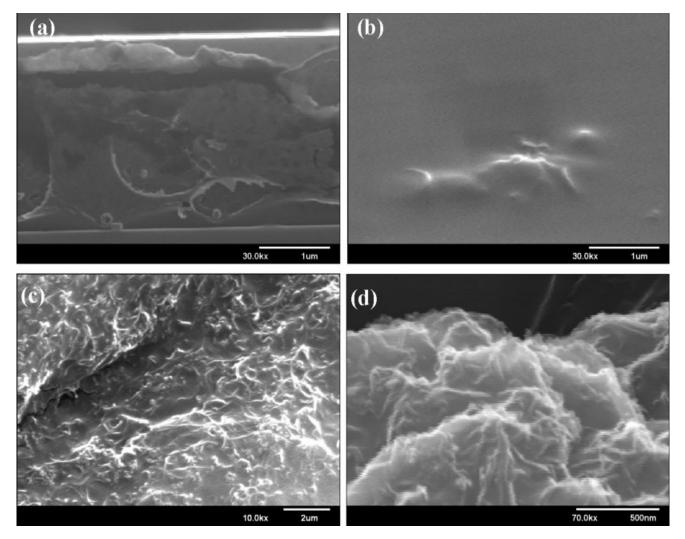
FIG. 2.   SEM images of (a) pure PMMA matrix, (b) surface image of MWCNT/PMMA composite, (c) fracture surface image of composite film, (d) large magnitude image of composite film.

their extreme flexibility [30]. Composite films were prepared by direct solution mixing. Sonicaiton at room temperature improved the dispersion properties. The interaction of the modified CNTs/PMMA nanocomposite is related to the carboxylate of the PMMA and the CNTs. The effective dispersion of fillers markedly increased the contact area, promoting the load transfer between the two components.

The mechanical properties, such as Young's modulus and hardness, were tested by the nanoindenter system. The elastic constant of sample was decided with non-axisymmetric indenters. The contact stiffness is obtained from the slope of the loading curve. An effective Young' modulus (E) is obtained by using the following equation [31–33].

$$S = \frac{dP}{dh} = C_A E A^{1/2}$$

where

$$\frac{1}{E} = \frac{1 - v_I^2}{E_I} + \frac{1 - v_S^2}{E_S}$$

where S is the contact stiffness, and it has the dimensions of force per unit distance. C_A is equal to $2/\sqrt{\pi}$, and A is the projected real contact area between the indenter and the surface. E_I and v_I are Young's modulus and poisson's ratio of the indenter, respectively. E_S and v_S are the same parameters of the test sample. The hardness of the surface (H) is determined by the equation $H = P/A$, where P is the loading force.

The load-displacement curve in Fig. 3 was utilized to determine the Young's modulus and hardness. During the experiment, the effect of the substrate must be determined. The mechanical scattering response depended on the filler of the matrix and increased on the CNTs content. A very homogeneous hybrid is obtained if both components are sufficient to create a good interpenetration of the two networks on the molecular scale. Hydrogen bonds are important interfacial forces, and are of two types in the composite system: intramolecular and intermolecular (such as OH···OH and OH···COOH). Carbonyl groups on the polymer macromolecules are strong acceptors of acidic hydrogen to form hydrogen bonds [34, 35].

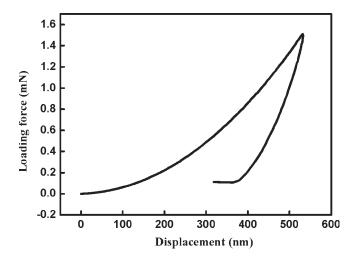Figure 4 plots the reduced modulus as a function tip displacement. The elastic modulus increased with CNT

FIG. 3. Typical loading force versus displacement curves obtained from the nanoindenter system.

FIG. 5. Effect of CNTs contents on the hardness and Young's modulus of composite films. [Color figure can be viewed in the online issue, which is available at www.interscience.wiley.com.]

contents. CNTs effectively strengthen the composite film. Figure 5 plots the Young's modulus and hardness of composites films with various carbon nanotube contents. The Young's modulus increased with the CNT content. However, the hardness increased to a maximum as the content of the CNTs increased to 2%, beyond which the hardness decreased. The stiffness associated with the treated CNTs that were dispersed effectively within the PMMA matrix caused the Young's modulus and hardness to increase with carbon nanotube content. The results indicated that the CNTs reinforced the mechanical strength of PMMA. Since CNTs have high aspect, high modulus, and high strength, the loading force can be transferred to the nanotubes. The load transfer also depends on the interfacial shear stress between the fiber and the matrix [36]. The main mechanisms of load transfer from matrix to filler are micromechanical interlocking, chemical bonding, and the Van Der Waals force [37].

Figure 6 presents the FTIR spectra of surface functional groups of nanocomposite films with various CNT contents. During polymerization, the functional group ($-OCH_3$) in the methyl methacrylate monomer was unchanged, but the $=CH_2$ functional group in the monomer was transformed to $-CH_2-$ [38, 39]. The C$-$O stretching vibration, which might be associated with an ester bond, ranged from 1100 to 1200 cm^{-1}. The C$-$H stretching vibration, which might be associated with the carbon of ethylene, is at 2850 to 3000 cm^{-1}. The peak at 1728 cm^{-1} is assigned to COO$^-$ [40]. The size of the phase separation between the filler and the matrix was varied from microns to the nanometers. A covalent interaction and the hydrogen bonds between PMMA and CNTs were desired to inhibit phase separation. The relative intensity of the hydrogen-bonded carbonyl group at 1715 cm^{-1} increased with the CNT content. The molecular structure did not obviously change after CNTs
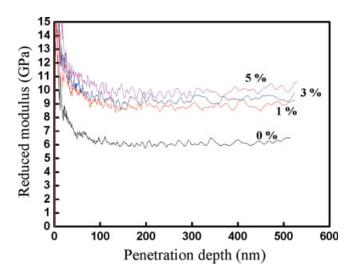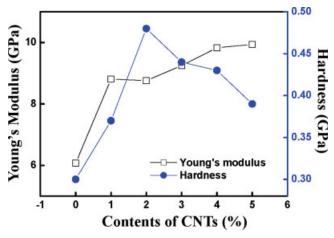

FIG. 4. Reduced modulus versus displacement curves of different CNTs contents on the CNTs/PMMA composite films. [Color figure can be viewed in the online issue, which is available at www.interscience.wiley.com.]
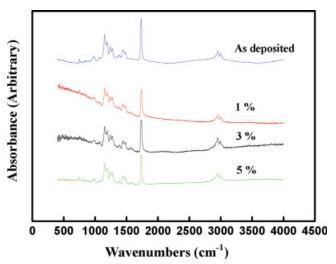

FIG. 6. FTIR spectrums of composite films with different contents of CNTs. [Color figure can be viewed in the online issue, which is available at www.interscience.wiley.com.]
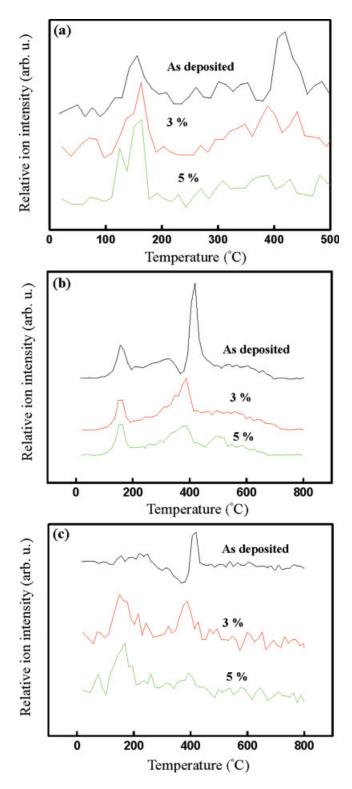
FIG. 7. Production of thermal desorption elements as a function of temperature with different contents of CNTs. (a) CH_3 (m/e = 15), (b) CO_2 (m/e = 44), and (c) O_2 (m/e = 32). [Color figure can be viewed in the online issue, which is available at www.interscience.wiley.com.]

were added to the PMMA matrix. The number of hydrogen atoms in the —OCH_3 groups of the composite film remained constant. The intensity of the carbonyl molecular group peaks increased when CNTs were added to the matrix, suggesting that the carbonyl groups in CNTs were covalently bonded to the PMMA matrix.

Figure 7a presents the outgassing behavior of —CH_3, desorbing from the surface of the composite film. The main desorption peaks were at 160 and 400°C. The desorption temperature of 160°C indicated that the thermal stability of PMMA is not high and composite films are destructive at this temperature. The intensity of desorption peak is reduced by adding CNTs. The carbon atoms at the surface are desorbed from the chain of σ bonds. The structure of PMMA comprises mainly carbon atoms. The addition of CNTs may cause the re-bonding of the dangling bonds. However, the exact configuration of the dangling bonds is not yet known.

Figure 7b shows the thermal desorption peaks of CO_2. CO_2 is formed at around 160°C. The sequence of the dispersion can be explained reasonably by the superposition of one-directional and normal-directional desorption. A CO_2 formation peak was observed because CO and oxygen reacted in the co-layer, as follows. CO molecules, which are produced by the desorption of methyl methacrylate on the surface of the film. The film was then further exposed to ambient oxygen. Following annealing, a CO_2 formation peak was formed because of the oxidation of CO. The amount of desorbed CO_2 depended on the CO coverage. The formation of CO_2 was suppressed as the CO coverage increased [41]. Figure 7c presents the thermal desorption properties of oxygen molecules. All curves exhibited a low-temperature peak at 100 to 250°C, and another peak at 380°C. At over 400°C, no desorption intensity was observed. The desorption spectra of pure PMMA and composite films varied significantly and extensively. The desorption peak at low temperature was observed because of physical desorption of gas from the surface. Consequently, the sites of adsorption depended on the chemisorbed oxygen, which diffused into the inner layer and saturated two neighboring dangling bonds with σ or π bonds. At high temperature, oxygen desorbs from the PMMA surface as CO_x, because of the thermal diffusion of recombined chemisorbed species, which results in second-order desorption and the formation of CO or CO_2 molecules.

CONCLUSION

In this study, direct mixing and sonication were adopted to prepare CNTs/PMMA composite films. CNTs were dispersed into the PMMA solution by acid treatment. The FTIR image revealed that carboxyl acid was bonded to the surfaces of CNTs and had a strong effect on dispersion performance. The nanoindenter test indicated that the Young's modulus and hardness increased as CNTs were added to the PMMA matrix.

REFERENCES

1. Y. Ishigure, S. Iijima, H. Ito, T. Ota, H. Unuma, M. Takahashi, Y. Hikichi, and H.J. Suzuki, *Mater. Sci.*, **34**, 2979 (1999).

2. M. Sumita, T. Shizuma, K. Miyasaka, and K. Ishikawa, *J. Macromol. Sci. Phys. B*, **22**, 601 (1983).

3. M. Sumita, T. Tsukurmo, K. Miyasaka, and K. Ishikawa, *J. Mater. Sci.*, **18**, 1758 (1983).

4. S.S. Ray and M. Biswas, *Synth. Met.*, **108**, 231 (2000).

5. A. Quivy, R. Deltour, A.G.M. Jansen, and P. Wyder, *Phys. Rev. B: Condens Matter*, **39**, 1025 (1989).

6. M.M.J. Treacy, T.W. Ebbesen, and J.M. Gibbson, *Nature*, **381**, 678 (1996).

7. Z. Yao, C.C Zhu, M. Cheng, and J. Liu, *Comput. Mater. Sci.*, **22**, 180 (2001).

8. M.F. Yu, B.S. Files, S. Arepalli, and R.S. Ruoff, *Phys. Rev. Lett.*, **84**, 5552 (2000).

9. R.E. Gorga and R.E. Cohen, *J. Polym. Sci. Part B: Polym. Phys.*, **42**, 2690 (2004).

10. Y. Sabba and E.L. Thomas, *Macromolecules*, **37**, 4815 (2004)

11. Z. Yang, B. Dong, Y. Huang, L. Liu, F.Y. Yan, and H.L. Li, *Mater. Lett.*, **59**, 2128 (2005).

12. Z. Jia, Z. Wang, C. Xu, J. Liang, B. Wei, D. Wu, and S. Zhu, *Mater. Sci. Eng. A*, **271**, 395 (1999).

13. H. Hu, B. Zho, K. Kamaras, and M.E. Itkis, *J. Am. Chem. Soc.*, **125**, 14893 (2003).

14. J. Chen, H. Liu, W.A. Weimer, M.D. Halls, D.H. Waldeck, and G.C. Walter, *J. Am. Chem. Soc.*, **124**, 9034 (2002).

15. H. Kuzmany, A. Kukovecz, F. Simon, and T. Pichler, *Synth. Met.*, **141**, 113 (2004).

16. E.T. Thostenson and T.W. Chou, *Compos. Sci. Technol.*, **61**, 1899 (2002).

17. M.J. O'Connell, P. Boul, L.M. Ericson, C. Huffman, Y.H. Wang, E. Haroz, C. Kuper, J. Tour, K.D. Ausman, and R.E. Smalley, *Chem. Phys. Lett.*, **342**, 265 (2001).

18. V.C. Moore, M.S. Strano, E.H. Haroz, R.H. Hauge, R.E. Smalley, J. Schmidt, and Y. Talmon, *Nano. Lett.*, **3**, 1379 (2003).

19. M. Monthioux, B.W. Smith, B. Burteaux, A. Claye, J.E. Fischer, and D.E. Luzzi, *Carbon*, **39**, 1251 (2001).

20. L. Vaccarini, C. Goze, R. Aznar, V. Micholet, C. Journet, and P. Bernier, *Synth. Met.*, **103**, 2492 (1999).

21. S.C. Tsang, P.J.F. Harris, and M.L.H. Green, *Nature*, **362**, 520 (1993).

22. E. Dujardin, T.W. Ebbesen, A. Krishnan, and M.M.J. Treacy, *Adv. Mater.*, **10**, 611 (1998).

23. P.M. Ajayan, T.W. Ebbesen, T. Ichihashi, S. Iijima, K. Tanigaki, and H. Hiura, *Nature*, **362**, 522 (1993).

24. M.A. Hamon, J. Chen, H. Hu, Y. Chen, A.M. Rao, and P. Eklund, *Adv. Mater.*, **11**, 834 (1999).

25. H. Hiura, T.W. Ebbesen, and K. Tanigaki, *Adv. Mater.*, **7**, 275 (1995).

26. J. Chen, M.A. Hamon, H. Hu, Y. Chen, A.M. Rao, P.C. Eklund, and R.C. Haddon, *Science*, **282**, 95 (1998).

27. S. Niyogi, M.A. Hamon, H. Hu, B. Zhao, P. Bhowmik, R. Sen, M.E. Itkis, and R.C. Haddon, *Acc. Chem. Res.*, **35**, 1105 (2002).

28. J. Liu, A.G. Rinzler, H. Dai, J.H. Hafner, R.K. Bradley, and R.E. Smalley, *Science*, **280**, 1253 (1998).

29. J. Huang and R.B. Kaner, *J. Am. Chem. Soc.*, **126**, 851 (2004).

30. L.S. Schadler, S.C. Giannaris, and P.M. Ajayan, *Appl. Phys. Lett.*, **73**, 3842 (1998).

31. J. Mencik, D. Munz, E. Quandt, E.R. Weppelmann, and M.V. Swain, *J. Mater. Res.*, **12**, 2475 (1997).

32. A.K. Bhattacharya and W. Nix, *Int. J. Solids Struct.*, **24**, 1287 (1988).

33. M. Fukuhara and I. Yamauchi, *J. Mater. Sci.*, **28**, 4681 (1993).

34. C.J. Brinker and G.W. Scherrer, *Sol-Gel Science, the Physics and Chemistry of Sol-Gel Processing*, Academic Press, Boston (1990).

35. C.J.T. Landry, K.C. Bradley, J.A. Wesson, and J.L. Lippert, *Polymer*, **33**, 1496 (1992).

36. G. Tsagaropoulos and A. Eisenberg, *Macromolecules*, **28**, 6067 (1995).

37. K. Liao and S. Li, *Appl. Phys. Lett.*, **79**, 4225 (2001).

38. C.C.C Ma and C.H Chen, *J. Appl. Polym. Sci.*, **44**, 807 (1992).

39. C.C.C Ma and C.H Chen, *J. Appl. Polym. Sci.*, **44**, 819 (1992).

40. S.W. Wee and S.M. Park, *Bull. Korean Chem. Soc.*, **22**, 914 (2001).

41. T. Matsushima, *Heterogeneous Chem. Rev.*, **2**, 51 (1995).